

# Non-resonant optical control of a spinor polariton condensate

A. Askitopoulos,<sup>1,\*</sup> K. Kalinin,<sup>2</sup> T.C.H. Liew,<sup>3</sup> P. Cilibrizzi,<sup>1</sup> Z. Hatzopoulos,<sup>4,5</sup> P.G. Savvidis,<sup>4,6</sup> N.G. Berloff,<sup>2,7</sup> and P.G. Lagoudakis<sup>1,†</sup>

<sup>1</sup>*Department of Physics & Astronomy, University of Southampton, Southampton, SO17 1BJ, United Kingdom*

<sup>2</sup>*Skolkovo Institute of Science and Technology Novaya St., 100, Skolkovo 143025, Russian Federation*

<sup>3</sup>*School of Physical and Mathematical Sciences,*

*Nanyang Technological University, 637371, Singapore*

<sup>4</sup>*Microelectronics Research Group, IESL-FORTH, P.O. Box 1527, 71110 Heraklion, Crete, Greece*

<sup>5</sup>*Department of Physics, University of Crete, 71003 Heraklion, Crete, Greece*

<sup>6</sup>*Department of Materials Science and Technology, University of Crete, Crete, Greece*

<sup>7</sup>*Department of Applied Mathematics and Theoretical Physics,*

*University of Cambridge, Wilberforce Road, Cambridge CB3 0WA, UK*

(Dated: May 12, 2016)

We investigate the spin dynamics of polariton condensates spatially separated from and effectively confined by the pumping exciton reservoir. We obtain a strong correlation between the ellipticity of the non-resonant optical pump and the degree of circular polarisation (DCP) of the condensate at the onset of condensation. With increasing excitation density we observe a reversal of the DCP. The spin dynamics of the trapped condensate are described within the framework of the spinor complex Ginzburg-Landau equations in the Josephson regime, where the dynamics of the system are reduced to a current-driven Josephson junction. We show that the observed spin reversal is due to the interplay between an internal Josephson coupling effect and the detuning of the two projections of the spinor condensate via transition from a synchronised to a desynchronised regime. These results suggest that spinor polariton condensates can be controlled by tuning the non-resonant excitation density offering applications in electrically pumped polariton spin switches.

PACS numbers:

## I. INTRODUCTION

Implementation of all optical, integrable spin-polarization switching devices is one of the essential ingredients for the realisation of novel solid state optoelectronic spin-logic architectures [1]. Semiconductor microcavities operating in the strong coupling regime, have recently emerged as ideal systems for achieving this goal due to their inherent spin multi-stabilities [2, 3] and fast spin dynamics [4, 5] that arise from their strong optical non-linearities [6]. Exciton-polaritons, the eigenstates of these systems, are bosonic light-matter quasiparticles that inherit the spin properties of their exciton component while their decay gives rise to photons with a polarization defined by the polariton spin. This robust spin to photon polarization conversion is favourable for fast non-destructive readout of the spin state of the system. Moreover, the advancement of fabrication techniques has yielded microcavity structures of high finesse featuring polariton lifetimes of the order of tens of picoseconds [7], enabling the emergence of optically excited polariton lasing and condensation [8, 9] even at room temperature [10]. In state of the art microcavity structures, polariton condensates propagate ballistically [11] and this has enabled the first demonstrations of polariton condensate optical switches [12–14].

Initial realizations of resonant polariton spin-switches [15], followed by experimental demonstrations of extensive polariton spin transport in planar [16] as

well as 1D structures [17], has emphasized the potential of theoretical propositions for fully integrated polariton based spin circuits [18, 19]. The short lifetime of polaritons considered to be an impediment for thermodynamic equilibrium and bosonic condensation can now be seen as an advantage in creating ultra-fast spin switching devices. In this regard, as non-resonant excitation schemes more closely resemble polariton formation under electrical injection, they hold greater promise for the implementation of electrically controlled polariton spin logic devices. This remarkable possibility has been further highlighted by the recent development of novel electrically pumped polariton lasers [20, 21].

In polarization resolved experiments under resonant excitation [15], parametric amplification [4] as well as in the OPO configuration [5, 22], correlations between the polarization of the excitation beam and the resulting polariton spin have been extensively studied. For non-resonant excitation, prior studies have demonstrated that upon condensation, the polarization of the condensate is pinned to the crystallographic axis of the microcavity structure independent of the exciting polarization [23]. This effect has been originally attributed to a linear polarization splitting of  $\approx 0.1\text{meV}$  (at  $k_{\parallel} = 0$ ), disputing that the emission polarization is inherited from the excitation [23]. The spontaneous emergence of a strong linear polarization upon condensation threshold has in-fact been treated as a suitable order parameter for determining the emergence of coherence in the system [24, 25].

However, in more recent experiments, a higher total degree of polarization was reported under circularly polarised non-resonant pulsed excitation rather than for linearly polarised excitation [26]. Moreover in polariton spin textures generated under circularly polarised excitation a high DCP was reported in the vicinity of the pump spot [16, 17]. These experiments confirmed that there are correlations between the polarisation of the optical excitation with the polarisation of the condensate, which in GaAs/AlGaAs MCs are not screened from optical disorder.

In this letter, we demonstrate that the spin imbalance in a polariton condensate can be vigorously modulated by the polarization properties of the non-resonant excitation beam when the polariton condensate and excitation reservoir are spatially separated. In the non-linear regime we observe a strong linear to circular polarisation conversion controlling the condensate polarization by tuning the angle of the linear polarization of the excitation beam. Moreover, the condensate density is shown to strongly effect the resulting spin imbalance leading to a spin reversal at high densities. We explain this reversal within the framework of a coherent internal Josephson coupling mechanism between the overlapping spin states of the condensate and present results of analytical approximations and numerical simulations that closely reproduce the experiment. These experiments confirm that the polarization of non-resonant excitation indeed survives the relaxation mechanisms from electron and holes to polaritons and its effects are exacerbated when the strong interactions from the reservoir are spatially decoupled. Furthermore, internal Josephson coupling effects between spin up and spin down coherent states are demonstrated to be an important factor governing the polarization build up in the condensate.

## II. EXPERIMENTAL RESULTS

To study the polarization properties of a polariton condensate we utilize the optical trap configuration from our previous work [27]. Using a non-resonant continuous wave (CW) linearly polarized pump spatially shaped in the form of an annular ring and focused on the sample surface through a 0.4 numerical aperture (NA) objective, we create the  $\Psi_{00}$  coherent state in the optically induced trap, as shown schematically in Fig.1a [28]. The  $S_+$  and  $S_-$  components of the emission below and above threshold are resolved with the use of a  $\lambda/4$  wave-plate and a linear polariser and are then used to reconstruct a real space image of the  $S_z$  stokes component [29]. We used a high Q (16000)  $5\lambda/2$  microcavity with a cavity lifetime of  $\sim 7ps$  composed of GaAs/AlGaAs DBRs, while the cavity is embedded with four triplets of 10nm GaAs quantum wells with  $Al_{0.3}Ga_{0.7}As$  barriers.

Below threshold we do not detect any significant cir-

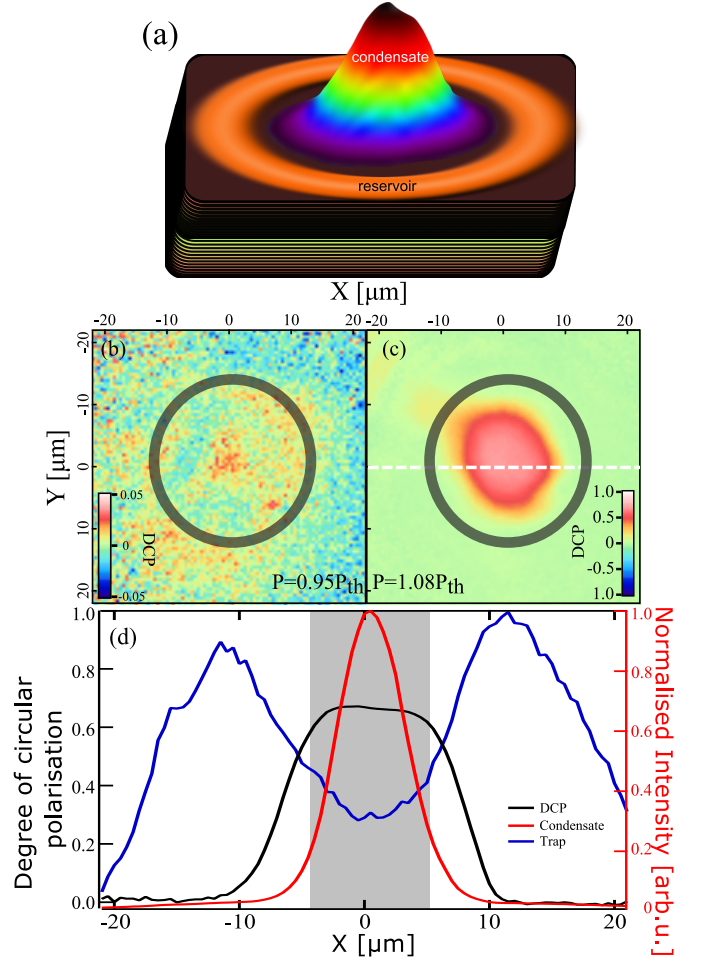


FIG. 1: (a) Schematic representation of reservoir and condensate in the microcavity. Real space map of the degree of circular polarisation (b) below ( $P = 0.95P_{th}$ ), and (c) above ( $P = 1.08P_{th}$ ) condensation threshold. (d) Normalised intensity of the polariton emission above threshold (red line, right axis), below threshold (blue line, right axis) and DCP (black line, left axis) across the white dotted line profile of (c).

cular polarization from polaritons inside the trap, shown on Fig.1b, however, just above the threshold we detect a strong circularly polarised emission of about 0.6 DCP as shown in Fig.1c. This is in stark contrast with the linear polarization build-up previously reported for polariton condensates [23]. It is worth noting that the circular component originates from the emission of the condensate while the DCP of the surrounding excitation region, where polaritons interact with the incoherent reservoir is negligible. Interestingly, this strong  $S_z$  stoke component persists far from the peak of the condensate and exhibits a  $DCP > 0.5$  even where the condensate intensity is 10% of its peak intensity as shown in Fig.1d.

Although the emergence of a strong spin imbalance from a linearly polarized optical pump appears counter intuitive, it can nevertheless be interpreted if one takes into account that the polarization of a monochromatic tightly focused optical field does not have a uniform po-

larization. For high numerical aperture lenses, scalar diffraction geometry is insufficient to accurately describe the electromagnetic field in the focal plane and a vectorial analysis of light is required in order to precisely describe the electromagnetic field in the focal plane [30]. Indeed it is a well studied effect that the electric field in the focal plane of a high numerical aperture aplanatic system can induce a small degree of ellipticity even for a 100% linearly polarized source [31, 32]. In our setup, the microscope objective (NA= 0.4), yields a measured DCP at the center of a focused linearly polarized beam of 0.1 [33]. Moreover, this ellipticity is calculated to be greater towards the periphery of the focal plane, where our ring-like excitation pattern is found, than in the central region [30].

The ellipticity of the pump does not play an important role below threshold where the emission is stronger in the excitation region. Indeed, it has been predicted that spin noise fluctuations are extremely sensitive to the statistics and occupation number in polariton systems [34]. Therefore, in the incoherent state a small spin imbalance (pump with small ellipticity) in the injection of carriers is not expected to have a noticeable effect in the polarisation of the emission. This has been demonstrated even for fully circular optical excitation schemes [26]. However, upon crossing the condensation threshold, a drastically different picture emerges. Spin fluctuations are greatly suppressed [34] and density dependent bosonic amplification favours the polariton spin state with higher occupation. In the absence of any spin relaxation mechanism between  $S_{\uparrow}$  and  $S_{\downarrow}$  polaritons, the bosonic amplification of the dominant spin population gives rise to a strongly circularly polarised polariton condensate. Furthermore, the spatial separation of the condensate from the exciton reservoir amplifies this behaviour as the spin decoherence channels associated with polaritons interacting with particles within the reservoir are considerably suppressed [27]. In excitation schemes where the reservoir is spatially overlapped with the condensate (e.g. top hat or Gaussian spot excitation) the scattering processes within the reservoir suppress externally imposed spin imbalances. However even in such cases, careful analysis of the spatiotemporal polarisation dynamics have shown spin phenomena that are driven by the spin imbalance in the exciton reservoir, such as polariton spin whirls and intricate spin textures [33, 35].

In order to further characterise the origin of the circular polarization in the condensate it is meaningful to establish whether it is isotropic and independent of the angle of the linear polarization of the optical pump. To achieve this, we initialize the condensate above threshold ( $P = 1.1P_{th}$ ) as before and using a half wave-plate we rotate the linear polarisation of the excitation. Figure 2(a) displays the spatial profile of the DCP under horizontal ( $0^\circ$ ) linear excitation showing a high DCP in the emission. Rotating the angle initially has a marginal

effect on the circular stokes component of the condensate. However, for polarization rotation above  $90^\circ$ , the DCP is reduced eventually leading to a complete reversal of the polarisation at  $130^\circ$  as shown in Fig. 2(b). After  $180^\circ$  rotation of the linear polarisation angle the condensate has regained its original polarisation. Figure 2(c) shows the spatial DCP near the tipping point. In this regime it has been shown that individual realizations of the trapped condensate are stochastically spin up or spin down [36]. Furthermore, perturbation of the system by a polarised femtosecond pulse can also induce temporary as well as permanent spin flips [36, 37], depending on the polarization of the pulse and of the trapped condensate. The DCP of the system has almost a  $2\theta$  relation with the angle of the linear polarisation of the excitation, shown in Fig. 2(d), where the value of each point is the average of the DCP in the central region of the condensate.

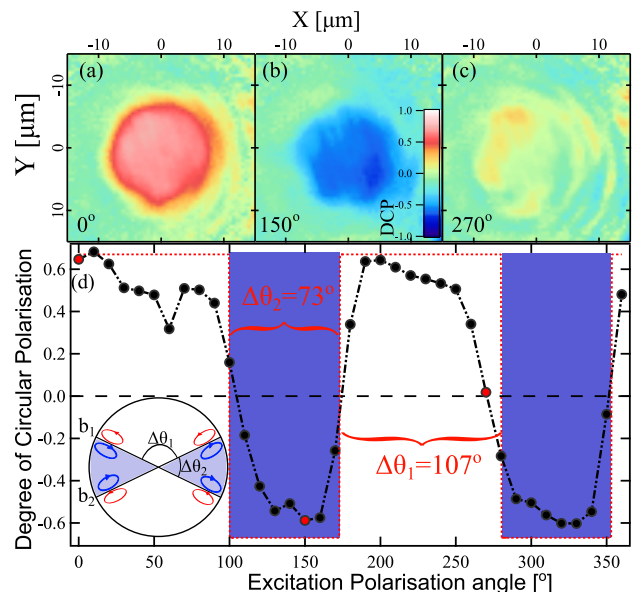


FIG. 2: Variation of the condensate's DCP with the linear polarisation angle of the excitation beam. Circular polarisation maps of the confined polariton condensate just above threshold for linear polarisation angle: (a)  $\theta = 0^\circ$ , (b)  $\theta = 150^\circ$  and (c)  $\theta = 270^\circ$ . (d) The average DCP is plotted versus external polarisation angle featuring a  $2\theta$  dependence (red dots mark the data at the above angles. Inset: schematic representation of the induced ellipticity to the excitation beam vs the linear polarisation angle.

The demonstrated  $2\theta$  dependence on the angle of the excitation polarization is an indication of optical anisotropy present in the sample. Light focused on the surface of the sample propagates through the top DBR mirror, where there is no absorption for the excitation wavelength ( $\lambda_{laser} = 752nm$ ), before exciting the excitons in the QWs. In our sample the DBR consists of pairs of AlAs/ $Al_{0.3}Ga_{0.7}As$  layers for which there have been a number of works, for similar multi-layered structures reporting linear birefringence [38–40]. The birefrin-

gence in the DBR will therefore exacerbate the ellipticity of the excitation beam and result in the  $2\theta$  dependence. Therefore the observed symmetry breaking at threshold is explicit (brought about by the imbalance in the population of  $S_{\uparrow,\downarrow}$  particles), except for the narrow region of polarization angles that the switching is observed.

In the previously discussed results, the excitation power of the non-resonant, non-local pump and therefore the condensate density was kept constant ( $P=1.1 \times P_{th}$ ). In polariton condensates, increasing the density has been shown to have a strong impact on its polarization through the increase of spin dependent polariton-polariton interactions that tend to depolarize the emission [26, 41]. We investigate the condensate density dependence in a polarization resolved power dependent experiment. Further increase of the density above threshold initially results in reducing the DCP of the emission. However at 2.2 times the threshold power we observe a reversal of the DCP and thus of the polariton pseudo-spin Fig. 3(a). It is worth noting here that we do not observe any deviation from the ground state of the trap within the power range that we studied. This is demonstrated in the inset of Fig. 3(a) that shows the real space 1D profile of the 2 spin components of the condensate with respect to power over threshold. Figure 3(b) depicts the power dependence of a spatial cross-section of the emission for increasing power, while the black line denotes the photoluminescence from the trap barriers below threshold that outlines the trap profile. The points of Fig. 3(a) are taken from the point of maximum intensity of the condensate ( $I_{\uparrow} + I_{\downarrow}$ ). Due to the intensity non-linearity, inherent in polariton condensation, the signal to noise ratio (SNR) that we record from the reservoir region, which is below threshold, is much greater than that at the centre of the trap ( $SNR_{res} \approx 0.1dB, 8.75dB \leq SNR_c \leq 14dB$ ). In Figure 3(b) we plot the DCP in the region of confidence where  $SNR \geq 1dB$ . The spin reversal dependence of a polariton condensate with excitation density under non-resonant optical pumping cannot be described within the framework of the linear optical spin Hall effect [42].

### III. JOSEPHSON COUPLING MODEL

Our theoretical model consists of a system of spinor Ginzburg-Landau equations (GLE) [43] written in the basis of left- and right-circular polarized polariton wavefunctions (spin-up and spin-down), denoted by  $\psi_{\pm}$ :

$$i\hbar \frac{\partial \psi_{\pm}}{\partial t} = \left\{ -\frac{\hbar^2}{2m} \nabla^2 + U_0 |\psi_{\pm}|^2 + (U_0 - 2U_1) |\psi_{\mp}|^2 + \hbar g_R n_{\pm} + \frac{i\hbar}{2} (R_R n_{\pm} - \gamma_C) \right\} \psi_{\pm} + \Omega \psi_{\mp}, \quad (1)$$

where in the Hamiltonian part of the equations we take into account an interaction with the total polariton den-

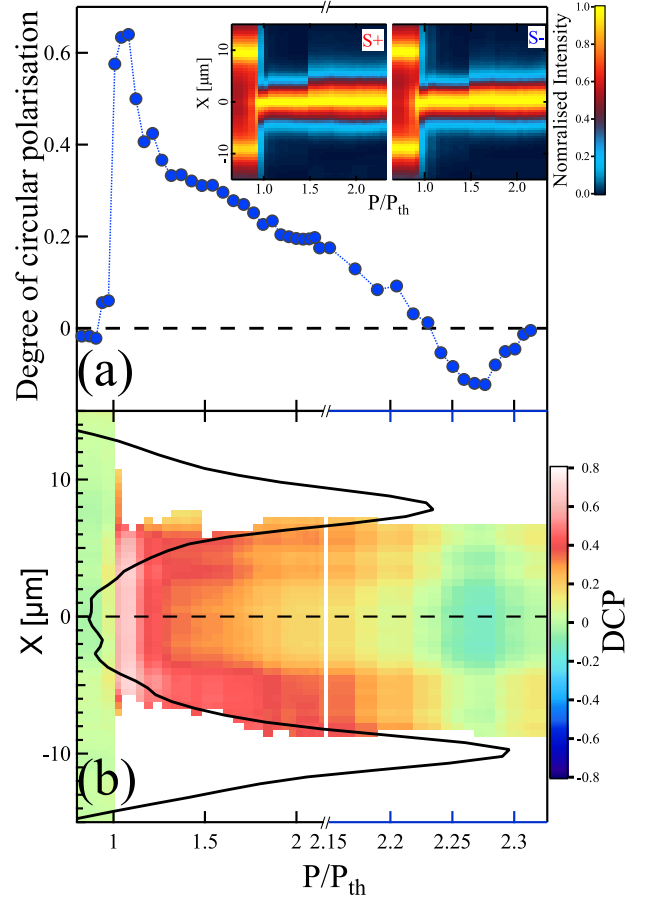


FIG. 3: (a) DCP as a function of excitation power vs threshold power. (b) Power dependence vs a spatial cross-section of the DCP across the trap. The figure shows the region where  $SNR \geq 1dB$ . The black line outlines the emission below threshold defining the trap. The inset in (a) shows the 2 spin components of the 1D real space profile of the condensate with respect to power above threshold.

sity  $H_{U_0} = U_0/2(|\psi_+|^2 + |\psi_-|^2)^2$  as well as an attractive interaction between opposite spin species,  $H_{U_1} = -2U_1|\psi_+|^2|\psi_-|^2$ , and the symmetry-breaking term  $H_{\Omega} = \Omega(\psi_+\psi_-^* + H.c.)$ , which arises due to asymmetry at the quantum-well interfaces, mechanical stresses, or due to the anisotropy-induced splitting of linear polarisations in the microcavity. Josephson coupling has been extensively studied and experimentally observed in polariton condensates, both in the intrinsic case [44, 45] as well as the extrinsic case [46–50]. In this model there is no explicit dependence on the shape of the pump, nevertheless the symmetry breaking term  $H_{\Omega}$ , appears exactly because the interactions with the reservoir are filtered out due to the geometry of the experiment [51]. The rate equation for the reservoir represents the evolution of the exciton densities,  $n_{\pm}$  is:

$$\frac{\partial n_{\pm}(\mathbf{r}, t)}{\partial t} = -(\gamma_R + R_R |\psi_{\pm}|^2) n_{\pm}(\mathbf{r}, t) + P_{\pm}(\mathbf{r}, t), \quad (2)$$



where we have neglected the hot excitons diffusion and advection. In equations 1 and 2,  $\gamma_R$  and  $\gamma_C$  are the reservoir and condensate decay rates respectively,  $R_R$  is the scattering rate to/from reservoir,  $P_{\pm}$  is the pumping rate and  $g_R$  is the condensate blueshift from interactions with reservoirs.

*Two-mode model.* We non-dimensionalize (1) and (2), neglect the spatial variation of all parameters and obtain the following ccGLEs and rate equations:

$$2i\frac{\partial\psi_{\pm}}{\partial t} = \{|\psi_{\pm}|^2 + (1 - U_{\alpha})|\psi_{\mp}|^2 + gn_{\pm} + \frac{i}{2}(Rn_{\pm} - 1)\}\psi_{\pm} + J\psi_{\mp}, \quad (3)$$

$$2\frac{\partial n_{\pm}}{\partial t} = -(\gamma + b|\psi_{\pm}|^2)n_{\pm} + p_{\pm}, \quad (4)$$

where the following dimensionless parameters were used [51]:

$$\begin{aligned} U_{\alpha} &= 2\frac{U_1}{U_0}; & g &= \frac{2mg_R}{\hbar}; & R &= \frac{2mR_R}{\hbar}; & J &= \frac{\Omega}{\hbar\gamma_C}; \\ \gamma &= \frac{\gamma_R}{\gamma_C}; & b &= \frac{\hbar R_R}{U_0}; & p_{\pm} &= \frac{\hbar}{2m\gamma_C^2}P_{\pm}. \end{aligned} \quad (5)$$

These equations can be conveniently re-parametrised using:

$$\psi_{\pm} = \sqrt{\rho_{\pm}}e^{i(\phi_{\pm}\frac{\Theta}{2})}, \quad \rho = \frac{\rho_+ + \rho_-}{2}, \quad z = \frac{\rho_+ - \rho_-}{2}, \quad (6)$$

where  $\rho_{\pm}$  are the densities of polaritons with spin-up and spin-down,  $\phi$  is the global phase which doesn't have an influence on our solution due to non-resonant incoherent pump,  $\Theta$  is the phase difference between the polaritons of different species,  $\rho$  is the averaged density. Separating real and imaginary parts gives the coupled equations for  $\Theta$ ,  $\rho$ , and  $z$ :

$$\begin{aligned} \dot{\Theta} &= -U_{\alpha}z - \frac{g}{2}(n_+ - n_-) + \frac{Jz \cos \Theta}{\sqrt{\rho^2 - z^2}}, \\ \dot{z} &= \frac{R}{4}(n_+(\rho + z) - n_-(\rho - z)) - J\sqrt{\rho^2 - z^2} \sin \Theta - \frac{z}{2}, \\ \dot{\rho} &= \frac{R}{4}(n_+(\rho + z) + n_-(\rho - z)) - \frac{\rho}{2}, \end{aligned} \quad (7)$$

where, in the view of the fast reservoir relaxation in comparison with the condensate relaxation ( $\gamma \approx 10$  [52–54]) we replaced Eq. (4) with the equilibrium values

$$n_{\pm} = \frac{p_{\pm}}{\gamma + b(\rho \pm z)}. \quad (8)$$

We are interested in the resulting degree of the circular polarization,  $\xi = z/\rho$ , assuming a small discrepancy in the pumping  $\eta = p_+/p_- > 1$ .

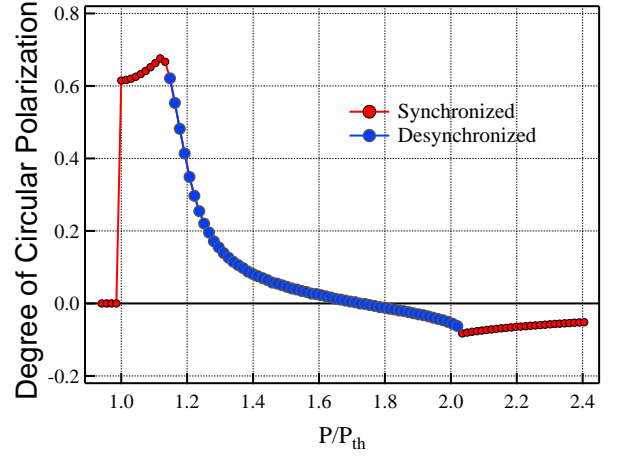


FIG. 4: The degree of circular polarization,  $\xi$ , as a function of the pumping strength  $P/P_{th}$  obtained by numerical integration of Eqs. (7). The blue dots correspond to the desynchronized state where the polarization degree and condensate density are oscillating in time (the values of these functions are averaged over the period of their oscillation), the red dots corresponds to fixed points. Even for a small discrepancy in the pumping intensity the degree of the circular polarization can vary from elliptical polarization to linear polarization to polarization reversal. The parameters used are  $\gamma = 10$ ,  $g = 0.7$ ,  $b = 15$ ,  $R = 1.0$ ,  $U_{\alpha} = 1.1$ ,  $J = 0.045$ ,  $\eta = 1.1$ .

*Josephson Regime.* The behaviour of the system (Eqs. 7) can be understood by considering the so-called Josephson regime:  $J \ll U_{\alpha}\rho$ ,  $z \ll \rho$ , and where we consider a small pumping discrepancy  $\eta = 1 + \epsilon$ , where  $\epsilon \ll 1$ . Eq. (7) reduces to an equation for a driven damped pendulum (or a current-based Josephson junction):

$$\begin{aligned} \ddot{\Theta} + \left( \frac{1}{2} - \frac{\gamma}{2Rp_-(1+\epsilon)} \right) \dot{\Theta} &= -U_{\alpha} \frac{\rho_{st}\epsilon}{2(2+\epsilon)} + \\ &+ J\rho_{st} \left( U_{\alpha} - \frac{gb}{(1+\epsilon)R^2p_-} \right) \sin \Theta, \end{aligned} \quad (9)$$

where the density  $\rho_{st}$  corresponds to the stationary case (a Bloch surface):

$$\rho_{st} = \frac{(\epsilon + 2)Rp_- - 2\gamma}{2b}. \quad (10)$$

The behaviour of the driven damped pendulum has been studied in detail [55]. Depending on the sign of the driving amplitude  $A = J\rho_{st}[U_{\alpha} - gb/(1+\epsilon)R^2p_-]$  the “pendulum” acts to drive  $\Theta$  to either 0 (if  $A > 0$ ) or to  $\pi$  (if  $A < 0$ ). The first term on the right-hand side of Eq. (10) represents a constant driving torque. The threshold condition for condensation is  $\gamma/Rp_- < 1$ , so the second term on the left-hand side of Eq. (10) represents damping with a rate  $\alpha = (1 - \gamma/Rp_-(1+\epsilon))/2$  that grows from the threshold approaching 1/2. We transform Eq. (10) into a set of the first order equations:

$$\dot{\Theta} = \chi, \quad \dot{\chi} = -\alpha\chi - U_{\alpha} \frac{\rho_{st}\epsilon}{2(2+\epsilon)} + A \sin \Theta. \quad (11)$$

From the analysis of this system it is clear that depending on the values of the coefficients the trajectory of the system is attracted to either a fixed point or a limit cycle. A stable fixed point exists if

$$U_\alpha \frac{\epsilon}{2(2+\epsilon)} \leq J|U_\alpha - \frac{gb}{(1+\epsilon)R^2 p_-}|. \quad (12)$$

We can refer to the corresponding fixed point solution as a synchronized solution since the relative phase of two components becomes fixed in time. If this condition is not satisfied, there is no fixed point and the relative phase between the components evolves periodically. We will refer to this regime as a desynchronized solution. The desynchronization occurs when Eq. (12) is violated which for small epsilon occurs when

$$\epsilon > 4J \left| 1 - \frac{gb}{U_\alpha R^2 p_-} \right|, \quad (13)$$

and in terms of the pumping takes place around

$$p_- \approx \frac{gb}{U_\alpha R^2}. \quad (14)$$

*Spin Reversal.* The presence of the internal Josephson coupling term,  $J$ , is essential for obtaining the spin reversal. If  $J = 0$  then the equation on the relative phase  $\Theta$  in Eqs. (7) becomes decoupled from the rest of the system. The regime for negligible  $J$  is relevant when the reservoir shields the condensate from the mechanical stresses and asymmetries of the underlying crystal (for instance for a single spot excitation). As the pumping strength grows the condensate enters the desynchronised regime which leads to small  $z$  getting close to the linearly polarized state. If  $J$  is non-zero, as one would expect for trapped condensates, the fixed point  $\dot{\Theta} = 0$  in the Josephson regime requires  $z$  to take negative values  $z \approx -g(n_+ - n_-)/2U_\alpha$ . Therefore, the transition from the synchronized regime at low pumping to desynchronised at higher pumping makes it possible for the system to reach the linear polarized state. The transition to a steady state is not possible without polarization spin flip. To verify this analysis we integrate Eqs. (7) and show the dependence of the DCP,  $\xi$ , on the pumping strength,  $p = p_-$ , over the threshold in Fig. 4).

#### IV. FULL SYSTEM

Finally, we check the dynamics of the DCP for a trapped condensate without neglecting the spatial variation. We solve

$$2i \frac{\partial \psi_\pm}{\partial t} = \{ -\nabla^2 + |\psi_\pm|^2 + (1 - U_\alpha)|\psi_\mp|^2 + gn_\pm + \frac{i}{2}(Rn_\pm - 1) \} \psi_\pm + J(\mathbf{r})\psi_\mp, \quad (15)$$

$$n_\pm(\mathbf{r}) = \frac{p_\pm(\mathbf{r})}{\gamma + b|\psi_\pm|^2}, \quad (16)$$

where the pumping profile,  $p_-$ , and the internal Josephson coupling,  $J$ , are given by

$$p_-(\mathbf{r}) = P \exp[-\alpha(r - r_0)^2], \quad (17)$$

$$J(\mathbf{r}) = \min(J_{\max}, 1/p_-).$$

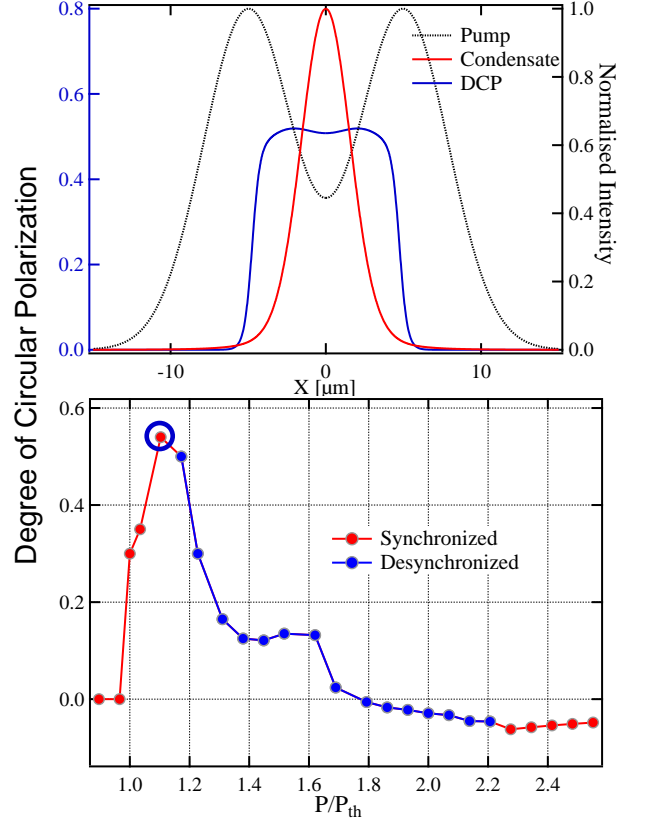


FIG. 5: (a) Simulated pump (dotted black line, right axis) and condensate (solid red line, right axis) real space profile plotted together with the condensate DCP profile (solid blue line, left axis) for  $P_{th}=1.1$  that has been multiplied by an appropriate hyperbolic tangent function to avoid the irrelevant DCP behaviour for the points where the condensate density is too small (less than  $10^{-2}$ ). (b) DCP,  $\xi$ , as a function of  $P/P_{th}$  for a trapped condensate pumped in a ring. The red points correspond to the fixed points, while the blue points to the averaged values of the desynchronized solutions. The blue circle in (b) denotes the point from where the profiles presented in (a) are extracted. Parameters are  $\gamma = 10$ ,  $g = 0.7$ ,  $b = 15$ ,  $R = 1.0$ ,  $U_\alpha = 1.1$ ,  $J_{\max} = 0.07$ ,  $\eta = 1.05$ ,  $\alpha = 0.06$ ,  $r_0 = 5$ .

The resulting condensate profile and DCP for a single power density, as well as the pump profile used are presented in Fig. 5(a). In Fig. 5(b) we show the dependence of the DCP,  $\xi$ , on the pumping strength above the threshold  $P/P_{th}$  for a condensate pumped in a ring. The solution was obtained by numerically solving system (15) for different  $P$  and using the spatial averaging of densities across the condensate. The initial pump spin discrepancy

was assumed to be 5% ( $\eta = 1.05$ ). The full 2D simulations support the conclusions of Section III. The system starts at a synchronized state for small pumping with a high DCP. The desynchronized regime brings the system closer to the linearly polarized state. The synchronized state at high pumping gives the polarization reversal according to the analysis of fixed points of Section III.

## V. CONCLUSIONS

We demonstrate the density dependence of the spin state of a polariton condensate under non-resonant optical excitation. We utilise the spatial separation of the exciton reservoir from the polariton condensate in an annular optical trap scheme, and show the emergence of a strongly polarised spinor condensate. The latter we attribute to the inherent spin imbalance induced by optical excitation in combination with the suppression of spin relaxation through scattering with the exciton reservoir. Most interestingly we observe a density dependent non-linear spin reversal at moderate optical excitation densities. The non-linearity of polariton spin dynamics is described and theoretically reproduced by introducing an internal Josephson coupling term in the spinor GLE, where the dynamics of the system are reduced to a current-driven Josephson junction. We show that the observed spin reversal is due to the interplay between an internal Josephson coupling effect and the detuning of the two projections of the spinor condensate via transition from a synchronised to a desynchronised regime. These results facilitate the design and implementation of polariton based non-linear spinoptronic devices such as electrically pumped polariton spin switches.

## ACKNOWLEDGEMENTS

P.G.L. acknowledges support by the Engineering and Physical Sciences Research Council of UK through the Hybrid Polaritonics Programme Grant (EP/M025330/1). P.G.S. acknowledges funding from the EU Social Fund and Greek National Resources (EPEAEK II, HRAKLEITOS II), N.G.B. acknowledges the financial support by Ministry of Education and Science of Russian Federation 1425320 (Project DOI: RFMEFI58114X0006). The authors acknowledge fruitful discussions with Prof. Alexey Kavokin and Dr Hamid Ohadi. The data from this paper can be obtained from the University of Southampton e-Print research repository.

<sup>†</sup> correspondence address: [pavlos.lagoudakis@soton.ac.uk](mailto:pavlos.lagoudakis@soton.ac.uk)

- [1] Žutić, I., Fabian, J., and Das Sarma, S. *Reviews of Modern Physics* **76**(2), 323–410 April (2004).
- [2] Paraíso, T. K., Wouters, M., Léger, Y., Morier-Genoud, F., and Deveaud-Plédran, B. *Nature Materials* **9**(8), 655–660 (2010).
- [3] Gavrilov, S. S., Sekretenko, A. V., Novikov, S. I., Schneider, C., Höfling, S., Kamp, M., Forchel, A., and Kulakovskii, V. D. *Applied Physics Letters* **102**(1), 011104–011104–4 January (2013).
- [4] Lagoudakis, P. G., Savvidis, P. G., Baumberg, J. J., Whittaker, D. M., Eastham, P. R., Skolnick, M. S., and Roberts, J. S. *Physical Review B* **65**(16), 161310 April (2002).
- [5] Kavokin, A., Lagoudakis, P. G., Malpuech, G., and Baumberg, J. J. *Physical Review B* **67**(19), 195321 May (2003).
- [6] Savvidis, P. G., Baumberg, J. J., Stevenson, R. M., Skolnick, M. S., Whittaker, D. M., and Roberts, J. S. *Physical Review Letters* **84**(7), 1547–1550 February (2000).
- [7] Nelsen, B., Liu, G., Steger, M., Snoke, D. W., Balili, R., West, K., and Pfeiffer, L. *Physical Review X* **3**(4), 041015 November (2013).
- [8] Wertz, E., Ferrier, L., Solnyshkov, D. D., Senellart, P., Bajoni, D., Miard, A., Lemaître, A., Malpuech, G., and Bloch, J. *Applied Physics Letters* **95**(5), 051108 August (2009).
- [9] Cilibrizzi, P., Askitopoulos, A., Silva, M., Bastiman, F., Clarke, E., Zajac, J. M., Langbein, W., and Lagoudakis, P. G. *Applied Physics Letters* **105**(19), 191118 November (2014).
- [10] Christopoulos, S., von Högersthal, G. B. H., Grundy, A. J. D., Lagoudakis, P. G., Kavokin, A. V., Baumberg, J. J., Christmann, G., Butté, R., Feltin, E., Carlin, J.-F., and Grandjean, N. *Physical Review Letters* **98**(12), 126405 March (2007).
- [11] Adrados, C., Liew, T. C. H., Amo, A., Martín, M. D., Sanvitto, D., Antón, C., Giacobino, E., Kavokin, A., Bramati, A., and Viña, L. *Physical Review Letters* **107**(14), 146402 September (2011).
- [12] Gao, T., Eldridge, P. S., Liew, T. C. H., Tsintzos, S. I., Stavrinidis, G., Deligeorgis, G., Hatzopoulos, Z., and Savvidis, P. G. *Physical Review B* **85**(23), 235102 June (2012).
- [13] Ballarín, D., De Giorgi, M., Cancellieri, E., Houdré, R., Giacobino, E., Cingolani, R., Bramati, A., Gigli, G., and Sanvitto, D. *Nature Communications* **4**, 1778 April (2013).
- [14] Antón, C., Liew, T. C. H., Sarkar, D., Martín, M. D., Hatzopoulos, Z., Eldridge, P. S., Savvidis, P. G., and Viña, L. *Physical Review B* **89**(23), 235312 June (2014).
- [15] Amo, A., Liew, T. C. H., Adrados, C., Houdré, R., Giacobino, E., Kavokin, A. V., and Bramati, A. *Nature Photonics* **4**(6), 361–366 June (2010).
- [16] Kammann, E., Liew, T. C. H., Ohadi, H., Cilibrizzi, P., Tsotsis, P., Hatzopoulos, Z., Savvidis, P. G., Kavokin, A. V., and Lagoudakis, P. G. *Physical Review Letters* **109**(3), 036404 July (2012).
- [17] Antón, C., Morina, S., Gao, T., Eldridge, P. S., Liew, T. C. H., Martín, M. D., Hatzopoulos, Z., Savvidis, P. G., Shelykh, I. A., and Viña, L. *Physical Review B* **91**(7), 075305 February (2015).
- [18] Liew, T. C. H., Kavokin, A. V., and Shelykh, I. A. *Physical Review Letters* **101**(1), 016402 July (2008).

---

\* correspondence address: [alexis.askitopoulos@soton.ac.uk](mailto:alexis.askitopoulos@soton.ac.uk)

- [19] Espinosa-Ortega, T. and Liew, T. C. H. *Physical Review B* **87**(19), 195305 May (2013).
- [20] Bhattacharya, P., Xiao, B., Das, A., Bhowmick, S., and Heo, J. *Physical Review Letters* **110**(20), 206403 May (2013).
- [21] Schneider, C., Rahimi-Iman, A., Kim, N. Y., Fischer, J., Savenko, I. G., Anthor, M., Lermer, M., Wolf, A., Worschech, L., Kulakovskii, V. D., Shelykh, I. A., Kamp, M., Reitzenstein, S., Forchel, A., Yamamoto, Y., and Höfling, S. *Nature* **497**(7449), 348–352 May (2013).
- [22] Cuadra, J., Sarkar, D., Viña, L., Hvam, J. M., Nalitov, A., Solnyshkov, D., and Malpuech, G. *Physical Review B* **88**(23), 235312 December (2013).
- [23] Kasprzak, J., Richard, M., Kundermann, S., Baas, A., Jeambrun, P., Keeling, J. M. J., Marchetti, F. M., Szymańska, M. H., André, R., Staehli, J. L., Savona, V., Littlewood, P. B., Deveaud, B., and Dang, L. S. *Nature* **443**(7110), 409–414 September (2006).
- [24] Laussy, F. P., Shelykh, I. A., Malpuech, G., and Kavokin, A. *Physical Review B* **73**(3), 035315 January (2006).
- [25] Baumberg, J. J., Kavokin, A. V., Christopoulos, S., Grundy, A. J. D., Butté, R., Christmann, G., Solnyshkov, D. D., Malpuech, G., Baldassarri Höger von Högersthal, G., Feltin, E., Carlin, J.-F., and Grandjean, N. *Physical Review Letters* **101**(13), 136409 September (2008).
- [26] Ohadi, H., Kammann, E., Liew, T. C. H., Lagoudakis, K. G., Kavokin, A. V., and Lagoudakis, P. G. *Physical Review Letters* **109**(1), 016404 July (2012).
- [27] Askitopoulos, A., Ohadi, H., Kavokin, A. V., Hatzopoulos, Z., Savvidis, P. G., and Lagoudakis, P. G. *Physical Review B* **88**(4), 041308 July (2013).
- [28] Askitopoulos, A., Liew, T. C. H., Ohadi, H., Hatzopoulos, Z., Savvidis, P. G., and Lagoudakis, P. G. *Physical Review B* **92**(3), 035305 July (2015).
- [29] Kavokin, K. V., Shelykh, I. A., Kavokin, A. V., Malpuech, G., and Bigenwald, P. *Physical Review Letters* **92**(1), 017401 January (2004).
- [30] Richards, B. and Wolf, E. *Proceedings of the Royal Society of London A: Mathematical, Physical and Engineering Sciences* **253**(1274), 358–379 December (1959).
- [31] Ha, T., Laurence, T. A., Chemla, D. S., and Weiss, S. *The Journal of Physical Chemistry B* **103**(33), 6839–6850 August (1999).
- [32] Lindfors, K., Friberg, A. T., Setälä, T., and Kaivola, M. *Journal of the Optical Society of America A* **22**(3), 561–568 March (2005).
- [33] Cilibrizzi, P., Sigurdsson, H., Liew, T. C. H., Ohadi, H., Wilkinson, S., Askitopoulos, A., Shelykh, I. A., and Lagoudakis, P. G. *Physical Review B* **92**(15), 155308 October (2015).
- [34] Glazov, M. M., Semina, M. A., Sherman, E. Y., and Kavokin, A. V. *Physical Review B* **88**(4), 041309 July (2013).
- [35] Cilibrizzi, P., Sigurdsson, H., Liew, T. C. H., Ohadi, H., Askitopoulos, A., Brodbeck, S., Schneider, C., Shelykh, I. A., Höfling, S., and Lagoudakis, P. *arXiv:1602.04711 [physics]* February (2016). arXiv: 1602.04711.
- [36] Ohadi, H., Dreismann, A., Rubo, Y., Pinsker, F., del Valle-Inclan Redondo, Y., Tsintzos, S., Hatzopoulos, Z., Savvidis, P., and Baumberg, J. *Physical Review X* **5**(3), 031002 July (2015).
- [37] Askitopoulos, A., Ohadi, H., Liew, T. C., Hatzopoulos, Z., Savvidis, P., Kavokin, A., and Lagoudakis, P. In *CLEO: 2014*, OSA Technical Digest (online), STu3O.3. Optical Society of America, June (2014).
- [38] Fainstein, A., Etchegoin, P., Santos, P. V., Cardona, M., Töttemeyer, K., and Eberl, K. *Physical Review B* **50**(16), 11850–11860 October (1994).
- [39] Sirenko, A. A., Etchegoin, P., Fainstein, A., Eberl, K., and Cardona, M. *physica status solidi (b)* **215**(1), 241–246 September (1999).
- [40] Ohke, S., Umeda, T., and Cho, Y. *Optics Communications* **70**(2), 92–96 February (1989).
- [41] Levrat, J., Butté, R., Christian, T., Glauser, M., Feltin, E., Carlin, J.-F., Grandjean, N., Read, D., Kavokin, A. V., and Rubo, Y. G. *Physical Review Letters* **104**(16), 166402 April (2010).
- [42] Kavokin, A., Malpuech, G., and Glazov, M. *Physical Review Letters* **95**(13), 136601 September (2005).
- [43] Borgh, M. O., Keeling, J., and Berloff, N. G. *Physical Review B* **81**(23), 235302 June (2010).
- [44] Gavrilov, S. S., Brichkin, A. S., Novikov, S. I., Höfling, S., Schneider, C., Kamp, M., Forchel, A., and Kulakovskii, V. D. *Physical Review B* **90**(23), 235309 December (2014).
- [45] Shelykh, I. A., Solnyshkov, D. D., Pavlovic, G., and Malpuech, G. *Physical Review B* **78**(4), 041302 July (2008).
- [46] Lagoudakis, K. G., Pietka, B., Wouters, M., André, R., and Deveaud-Plédran, B. *Physical Review Letters* **105**(12), 120403 September (2010).
- [47] Abbarchi, M., Amo, A., Sala, V. G., Solnyshkov, D. D., Flayac, H., Ferrier, L., Sagnes, I., Galopin, E., Lemaître, A., Malpuech, G., and Bloch, J. *Nature Physics* **9**(5), 275–279 May (2013).
- [48] Lien, J.-Y., Chen, Y.-N., Ishida, N., Chen, H.-B., Hwang, C.-C., and Nori, F. *Physical Review B* **91**(2), 024511 January (2015).
- [49] Christmann, G., Tosi, G., Berloff, N. G., Tsotsis, P., Eldridge, P. S., Zacharias Hatzopoulos, Savvidis, P. G., and Baumberg, J. J. *New Journal of Physics* **16**(10), 103039 (2014).
- [50] Solnyshkov, D. D., John, R., Shelykh, I. A., and Malpuech, G. *Physical Review B* **80**(23), 235303 December (2009).
- [51] Our dimensional parameters were  $\hbar\gamma_C = 0.1$  meV,  $\hbar\gamma_R = 1$  meV,  $\hbar R_R = 0.1$  meV  $\mu\text{m}^2$ ,  $U_0 = 0.0067$  meV  $\mu\text{m}^2$ , and  $\hbar g_R = 0.07$  meV  $\mu\text{m}^2$ .
- [52] Wouters, M., Carusotto, I., and Ciuti, C. *Physical Review B* **77**(11), 115340 March (2008).
- [53] Lagoudakis, K. G., Wouters, M., Richard, M., Baas, A., Carusotto, I., André, R., Dang, L. S., and Deveaud-Plédran, B. *Nature Physics* **4**(9), 706–710 September (2008).
- [54] Ge, L., Nersisyan, A., Oztog, B., and Tureci, H. E. *arXiv:1311.4847 [cond-mat, physics:nlin]* November (2013). arXiv: 1311.4847.
- [55] Strogatz, S. H. *Nonlinear Dynamics and Chaos: With Applications to Physics, Biology, Chemistry, and Engineering*. Westview Press, August (2008).